Ultrafast spectroscopy of coherent phonons across the pressure driven insulator to metal phase transition in V2O3

Thomas Gauthier, Nicolas Godin, Gaël Privault, Roman Bertoni, Etienne Janod, Danylo Babich, Benoit Corraze, Julien Tranchant, Laurent Cario

Ultrafast spectroscopy of coherent phonons across the pressure driven insulator to metal phase transition in V_2O_3

Thomas Gauthier, Nicolas Godin, Gaël Privault, and Roman Bertoni*
Univ Rennes, CNRS, IPR (Institut de Physique de Rennes) - UMR 6251, F-35000 Rennes, France

Etienne Janod, Danylo Babich, Benoit Corraze, Julien Tranchant, and Laurent Cario
Nantes Université, CNRS, Institut des Matériaux de Nantes Jean Rouxel, IMN, F-44000 Nantes, France

(Received 16 February 2024; accepted 5 August 2024; published 15 October 2024)

Nowadays, materials science is moving towards the understanding and control of materials in nonequilibrium states by making use of perturbative techniques to investigate their dynamical responses. From this perspective, the use of ultrashort light pulses seems to be a relevant approach as it can selectively address different degrees of freedom in solid-state systems and more particularly electrons. Such a method can help to decipher the physical phenomena arising from electronic correlations and complements a more conventional methodology where the phase diagrams of materials are investigated at thermodynamical equilibrium. Here, we combine femtosecond optical spectroscopy and a high-pressure setup to monitor the ultrafast out-of-equilibrium photo response of a V_2O_3 thin film across the pressure driven insulator-to-metal transition. The experimental results demonstrate the possibility to use the spectroscopy of coherent phonons as a thermodynamical phase marker in V_2O_3 thin films. In addition, the frequency behavior of the ultrafast coherent phonon mode (A_{1g} character) seems to reflect the manifestation of a strong coupling between the lattice and electronic degrees of freedom near first-order transition lines with a pronounced drop in frequency around the critical pressure.

DOI: 10.1103/PhysRevResearch.6.043037

I. INTRODUCTION

The Mott transition is one of the most fascinating phenomena in condensed matter physics [1,2]. This physical effect implies that a material that should be metallic considering its electronic band filling and atomic structure could present an electronic insulating phase induced by electronic correlations. Despite being discussed for more than 60 years, this effect still drags a tremendous amount of research and its global understanding is not fully covered yet. In its most simple picture, the Mott transition can be modeled with a simple Hubbard model considering only electronic bandwidth and on-site repulsion, accounting for correlations (often referred to as W and U, respectively). A common practice is to investigate the physics of Mott materials and their phase diagram by modulating the W parameter via the application of hydrostatic pressure. In this way, a Mott insulator can be turned into a correlated metal under increasing pressure. From that perspective, it is still a common dogma to consider the Mott transition under the sole aspect of electronic degrees of freedom and more specifically the U/W ratio. However, numerous studies have pointed out that, when approaching transition lines, electronic degrees of freedom couple to the lattice and more particularly to elastic degrees of freedom [3]. This coupling becomes even more relevant close to critical end points [4] where spectacular effects such as the breakdown of Hooke's law of elasticity can be observed [5]. Some complex models exist to include these degrees of freedom in the full physical picture of phase transitions in Mott materials [6–8]. These theoretical models suggest the emergence of this coupling in any measurements made near transition lines where the quantity probed experimentally is coupled to the elastic bulk modulus, and to the lattice at larger scales.

A prototypical Mott material is vanadium sesquioxide (V_2O_3), or its chromium-doped equivalent $(V_{1-x}Cr_x)_2O_3$, which can display a phase transition at room temperature between a paramagnetic insulating phase (PI) and a paramagnetic metallic phase (PM) under hydrostatic pressure [9]. This isosymmetric transition is accompanied by a large volume change revealing the strong coupling between electronic and lattice degrees of freedom. Furthermore, this structural change is also reflected in a variation of optical phonon frequencies with lower values in the PM phase. Indeed, according to previous Raman studies [10,11], a lower frequency of A_{1g} modes is observed in the metallic phase with a softening of a few percent compared to the ones of the PI phase.

On another aspect, the development of ultrafast laser-based technologies has granted access to strongly out-of-equilibrium states in solid-state materials at fundamental timescales for electronic and structural processes. It can be seen as a direct translation of the more conventional steady-state spectroscopy in the time domain where excited and nonthermal states can be

*Contact author: roman.bertoni@univ-rennes.fr

interrogated. Along this line, one of the most common techniques is ultrafast optical spectroscopy where an ultrashort optical pulse is used as an impulsive perturbation in order to investigate the response function of materials. One of the most singular effects in this field of research is the observation of coherent phonons, appearing as an oscillating temporal modulation of physical quantities such as the dielectric function or in diffraction patterns.

This process is often classified using two terminologies; displacive excitation of coherent phonon (DECP) [12] and impulsive Raman scattering (IRS) [13]. Both mechanisms can be described through a unifying Raman formalism and correspond to two limiting cases of the same physical process [14,15]. The case of DECP mostly refers to resonant excitation within the electronic band structure, which is often observed in semimetals (Bi, Sb) and semiconductors [12,16,17]. In this case, the electron-phonon coupling is responsible for the generation of a macroscopic number of optical phonons at the Brillouin zone center, the latter potentially probed by different techniques including optical spectroscopy and diffraction. When dealing with optical spectroscopy measuring simple optical quantities (reflectivity and transmission, for instance), only the totally symmetric modes of A, A_1 or A_{1g} characters are directly measurable. More recently, the study of nonequilibrium states by means of coherent phonon spectroscopy has been extended to numerous type of materials, including molecular materials [18–21], charge-density wave systems [22,23], transition-metal dichalcogenides [24–26], and transition-metal oxides including V_2O_3 [27–31]. Furthermore, the absence or presence of coherent phonons as well as their frequencies are a tool used nowadays to seek for the occurrence of photoinduced phase transition [32,33].

In the following, the idea we want to address is to scrutinize if the monitoring of ultrafast coherent phonons in a Mott material (V_2O_3) across an isosymmetric phase transition could provide some physical insights regarding its thermodynamical phase and dynamical response. In order to do so, we have measured the transient photoresponse of a V_2O_3 thin film across the pressure driven insulator-to-metal (IMT) phase transition at room temperature using ultrafast optical spectroscopy. By analyzing the transient reflectivity presenting the signature of coherent phonons, in which is embedded part of the lattice response, it is possible to observe the occurrence of the pressure driven Mott transition. In addition, the results display the presence of a strong coupling between the electronic subpart and the lattice inducing a pronounced softening of optical phonon near the critical pressure.

II. MATERIAL AND METHODS

A. Sample preparation

In this study, the sample under scrutiny is a thin film of pure V_2O_3 deposited on a SiO_2/Si substrate. After sputtering of a vanadium target in Ar/O_2 discharge, the sample is annealed at 1080 K for 10 h in a controlled atmosphere. The resulting sample is a centimeter square wide, single phase, V_2O_3 thin film of ∼200 nm thickness. Under cooling at ambient pressure (1 bar), this sample presents two transition temperatures

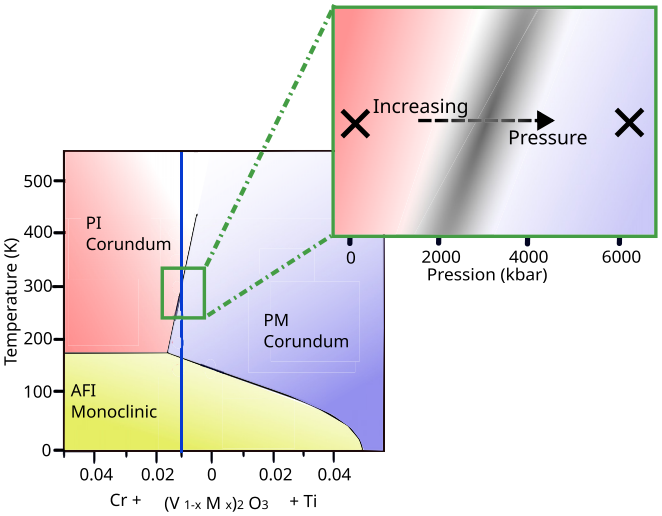

FIG. 1. Phase diagram of V_2O_3 adapted from Ref. [9]. The white area denotes the crossover region. The insert shows the expected path followed by the sample when hydrostatic pressure is applied. The blue line corresponds to the thermal path followed by the sample under cooling.

resulting in a double hysteresis loop. At room temperature, this sample is in the paramagnetic insulating (PI) phase with a corundum structure (space group $R\bar{3}c$). Upon cooling, it undergoes an isostructural phase transition towards the paramagnetic metallic phase (PM) at around 270 K. At an even lower temperature, a second phase transition to an antiferromagnetic insulating (AFI) phase occurs around 175 K. This transition is concomitant with a structural symmetry change from a corundum to a monoclinic structure. This peculiar thermal behavior is very likely due to the difference of thermal expansion between the SiO_2/Si substrate and V_2O_3, leading to a biaxial tensile strain after cooling down from 1080 K (annealing temperature) to room temperature. This dynamic is similar to the one displayed by bulk V_2O_3 substituted by 1% of Cr, as shown in the standard phase diagram of V_2O_3 (Fig. 1).

In the following, we focus our experimental investigation on the phase transition taking place at room temperature between the PI and PM phases; the isosymmetric Mott transition. According to a projected phase diagram (Fig. 1, insert) based on the thermal behavior of the sample (Fig. 8, Appendix B), the phase transition line should be crossed within 10000 bars (1 GPa) with an expected critical pressure between 2000 and 4000 bars.

B. Ultrafast optical spectroscopy

The ultrafast photoresponse of the sample is investigated by means of femtosecond optical spectroscopy. The methodology is based on the classical pump-probe scheme. An amplified Ti:sapphire femtosecond laser (7 mJ, 65 fs) operating at 1 khz is the core of the optical setup. A part of the out-coming pulse is split and sent on pump and probe beam paths. The probe beam is made of a supercontinuum pulse generated through a sapphire plate and covering the full visible range with a detection spanning from 475 nm (2.6 eV)

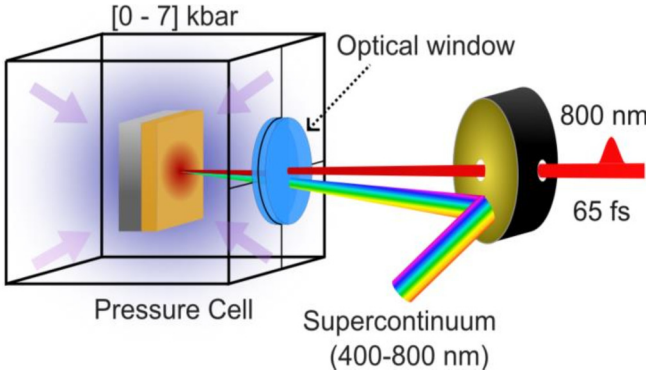

FIG. 2. Scheme of the experimental setup combining ultrafast optical spectroscopy and a high-pressure cell. The black lines represent the pressure cell area.

to 725 nm (1.7 eV). The detection scheme displays a global sensitivity of 2.10^{-5} for an averaging of 10000 spectra.

The pump photon energy is centered at 1.55 eV (800 nm) with an estimated pulse duration of ∼65 fs. This energy being much larger than the optical band gap of the PI phase, one expects to directly excite electrons above the gap. Thus, the interaction with the optical pump field results in a similar effect in both PI and PM phases with the ultrafast generation of an excited electronic gas [29]. The typical size (FWHM) of the pump pulse of quasi-Gaussian profile is around 290 μm leading to an average excitation density of 2.1 mJ/cm^2 (details of the calculation are provided in the Appendix). This value remains identical for all the data set presented afterwards.

We define the transient reflectivity discussed hereafter as:

$$\Delta R(t,\lambda) = \frac{R_{on}(t,\lambda) - R_{off}(\lambda)}{R_{off}(\lambda)} \quad (1)$$

with $R_{on}(t,\lambda)$ the reflectivity of the pumped material at a given delay t and $R_{off}(\lambda)$ the reflectivity of the unexcited material.

C. High-pressure cell

The scheme of the setup is displayed in Fig. 2. The high-pressure setup is based on a helium gas cell that can cover a pressure range from 1–7000 bar. The very large sample volume allows the study of thin systems of mm^2 size and mm thickness. The sample is mounted inside the cell, resulting in numerous optical interfaces inducing several reflected beams and providing an easy way to remove spurious contributions from the optical window. The use of a sapphire window ensures the possibility to operate in a spectral range spanning from 5–0.25 eV (250–5000 nm). Using this experimental configuration, we have performed ultrafast optical spectroscopy under hydrostatic pressure, from 1–6200 bar. Additional technical details can be found in Ref. [34]. All the measurements were collected on a single ramp of increasing pressure starting from ambient pressure. The very likely hysteretic behavior of the sample under pressure prevents comparing the case of compression and the decompression one.

III. RESULTS

We systematically measure transient broadband reflectivity changes as a function of the applied hydrostatic pressure after a femtosecond optical excitation with a 800 nm pump pulse. Figure 3 displays time-dependent broadband reflectivity obtained at 6200 bars. The presented data are corrected for the chirp of the supercontinuum probe, providing the same time axis for all wavelengths.

A clear oscillation modulating the full spectral range is observed up to 1.5 ps and is superimposed to a global photoinduced signal of ∼1% in absolute value. This feature, already reported in numerous studies [27–30,34], is attributed to the ultrafast generation of coherent phonons. The signal around time zero is strongly dominated by contributions resulting from nonlinear effects occurring in the sapphire optical window. This strong optical signature can be clearly seen in Fig. 4(a), where a complete time trace around the central wavelength of 675 nm is shown up to 1.5 ps. The plotted time trace is an average over a 25 nm wide spectral window in order to improve the statistics of the signal.

The experimental data are fitted by using a model containing three distinct components acting at different delays [Fig. 4(b)]. The details of this model are presented in Appendix A. First, a strong modulation of the signal is observed around time zero, with alternative positive and negative peaks. This feature is the signature of nonlinear optical effects [35–37] occurring both in the sapphire window and the sample, including cross-phase modulation (XPM). These effects are acting around time zero before the sample response and an additional fast electronic contribution might be present but is partially smeared out by these large nonlinear optical contributions (Fig. 7, Appendix A). Afterwards, a small oscillation lasting almost one picosecond is observed independently of the probed spectral range. The inset in Fig. 4(a), when an additional linear component is removed, provides a clear view of these oscillations. This oscillating component is fitted with an exponentially damped cosine, a conventional way for modeling coherent phonons [18,38]. Being only in PI or PM phases, we do expect to observe only one single phonon frequency related to the totally symmetric zone center A_{1g} mode [27,29]. This fitting method gives direct access to the frequency, the damping and the phase of the mode. These three quantities are relevant ones when discussing the physics of ultrafast coherent phonons. However, the correlation of

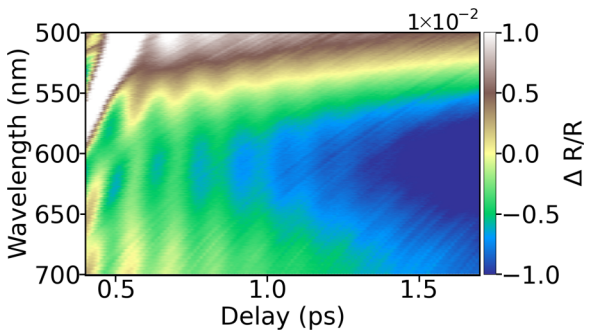

FIG. 3. Broadband transient variation of reflectivity following a 800 nm photoexcitation at 6200 bars.

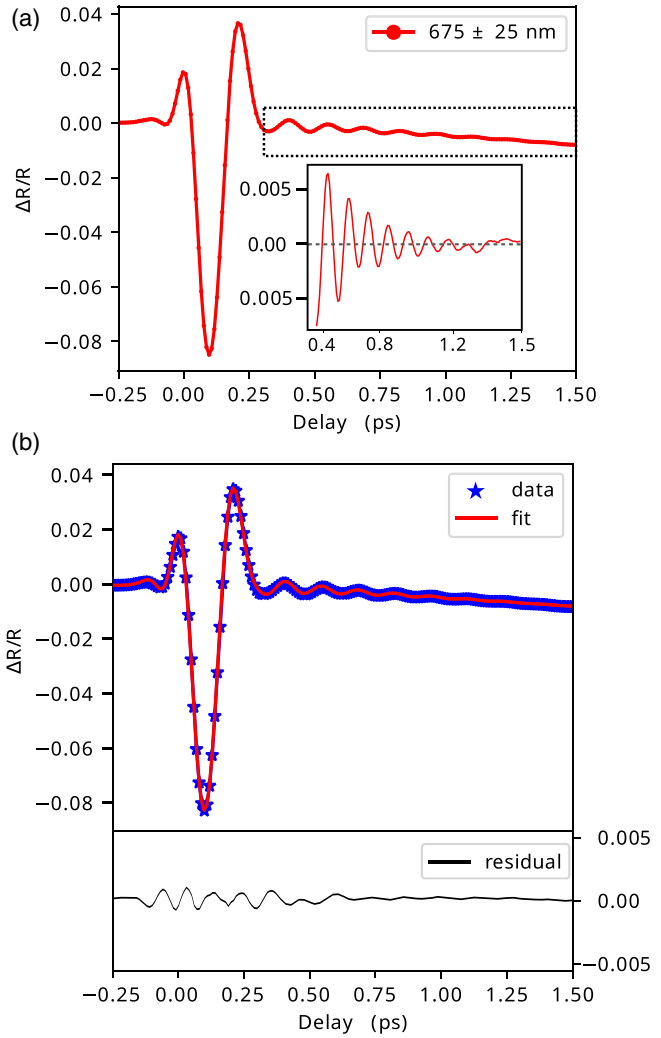

FIG. 4. (a) Transient reflectivity of a V_2O_3 thin film around 675 nm after photoexcitation with 800 nm pulse at 6200 bars. Insert is a zoom on the oscillating component. (b) Top, fit of the data accounting for nonlinear effects and coherent phonon. Raw data points are shown in blue and the fit in a red solid line. Bottom, residual component of the fit.

the phase parameter with other free parameters such as the experimental response function or the XPM component makes a reliable estimation of this quantity difficult. Nevertheless, the frequency and damping components are weakly correlated to the other free parameters, allowing for a complete study of their behaviors under hydrostatic pressure. This statement is supported by the fit shown in Appendix A where the artifact component (XPM) is removed from the global photoresponse (Fig. 7). Indeed, the signal related to coherent phonon is not affected by the XPM component, in contrast to a possible fast electronic response.

The fit shown in Fig. 4(b) (at 6200 bars) reveals a good agreement with the experimental data, and provides the following values: Frequency$(A_{1g}) = 7.14 \pm 0.02$ THz and damping-$\tau_d(A_{1g}) = 0.34 \pm 0.02$ ps. These values are consistent with previous studies performed on single crystals and thin film of V_2O_3 in the PM phase [29,30,39]. An additional component is added to account for slower

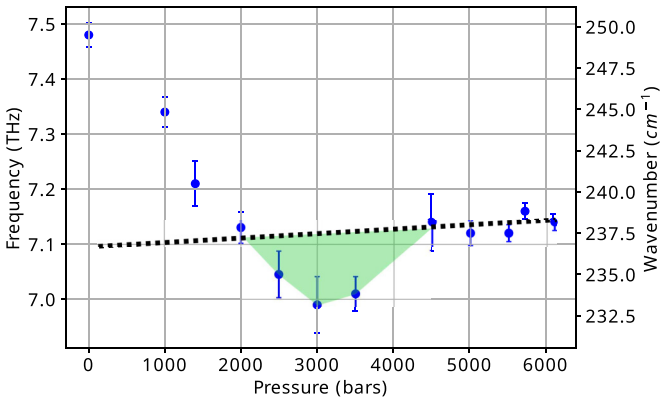

FIG. 5. Evolution of the fitted phonon frequency as a function of hydrostatic pressure. Dashed line represents an affine fit for values higher than 4500 bars. Error bars represent the standard deviation obtained from the fitting procedure.

dynamics that arise from thermoelastic effects. Such effects are related to the macroscopic response of the lattice and occur in the picosecond to nanosecond timescales, depending on the size of the sample [30,34]. Figure 5 shows the evolution of the extracted frequency as a function of the applied hydrostatic pressure. Every point is obtained using the same fitting method and keeping the same central probing wavelength (675 nm). This analysis reveals a dependency of the phonon frequency under pressure. First, the frequency seems to linearly decrease from 1 to 3000 bars. At this pressure, the frequency reaches a lower value of $\sim 7 \pm 0.05$ THz. It corresponds to a softening of $\sim 7\%$ compared to ambient pressure (~ 7.5 THz). This feature is consistent with the frequency shift of the A_{1g} mode observed during the pressure-induced PI-to-PM transition and monitored by Raman spectroscopy ($= 15$–20 cm^{-1}, i.e., 0.45–0.6 THz) (Fig. 9, Appendix C). As the pressure is further increased up to 4500 bar, the frequency increases slightly before reaching a plateau-like response with an average value of ~ 7.15 THz. Both phases undergo a shift of the A_{1g} phonon frequency under hydrostatic pressure. For the PM one, the experimental value of this shift is obtained by fitting the experimental points above 4500 bars with an affine function (dashed line). The average resulting coefficient is $+7.5 \times 10^{-3}$ THz per kbar. For the PI phase, the frequency shift is extracted from a Raman spectroscopy measurement on a PI single crystal (Fig. 9, Appendix C) and gives the experimental value of -9×10^{-3} THz per kbar. Even taking into account the coexistence of phases, which is very likely to occur during the pressure-induced transition, these values, extracted from the material far from the transition lines, cannot explain the abrupt softening of 0.5 THz over a region 3000 bar wide, as shown in Fig. 5, and the presence of a minimum at about 3000 bar. Indeed, this frequency has a lower value, between 2500 and 3500 bars, compared to the linear interpolation of a plausible high-pressure PM phase, highlighted by the green area in Fig. 5.

Regarding the damping component, all the fitted values are between 0.3 and 0.5 ps (gray area in Fig. 6), showing no obvious correlation with the applied hydrostatic pressure (Fig. 6).

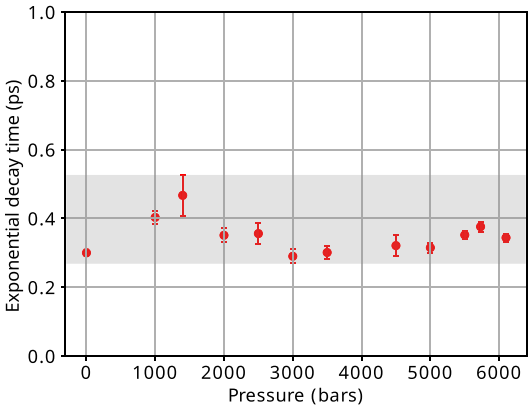

FIG. 6. Evolution of the fitted damping time as a function of hydrostatic pressure. Gray area emphasizes the observed range of decay time. Error bars represent the standard deviation obtained from the fitting procedure.

A persistent value of ~ 2 ps for the lifetime of coherent phonon at room temperature matches previous studies on this topic [28,29,39]. This suggests that the macroscopic phase of the system (PI or PM) does not strongly impact the damping dynamics of the coherent phonon. It indicates that the main damping mechanisms (electron-phonon and phonon-phonon scattering) are of similar order of magnitude in both PI and PM phases.

IV. DISCUSSION

The generation of coherent optical phonons upon ultrafast optical excitation is a well-known phenomenon [12,15]. The generated phonon, often in the THz range, is detectable using femtosecond optical pulses (100 fs ≈10 THz). The direct comparison between steady-state Raman spectroscopy and ultrafast coherent phonons is a common practice [27] but one should keep in mind that Raman spectroscopy is an incoherent effect probing the ground state of the material.

Related to the relaxation mechanism, it must be emphasized that most of the energy dissipation from the electronic subsystem toward the lattice occurs via an incoherent process. Only a very small amount of the initial excess energy is transferred directly to the lattice via the DECP mechanism. Overall, the main channel for dissipation remains electron-phonon scattering processes over the full Brillouin zone including acoustic branches [40,41]. The latter results in an temperature increase of the lattice. Here, the excitation density used for the experiment pushes the system far from equilibrium with an upper value of ≈ 25 K for heating effects in the thin film (see calculations in Appendix D).

The observation of coherent phonon in V_2O_3 has been described so far within the frame of the DECP mechanism because a genuine electronic excitation occurs while exciting the material with 1.5 eV photon energy [27,29,30]. This mechanism implies that the observed mode, when probing simple optical quantities, is a zone center Raman active mode with A_{1g} character. In both PI and PM phases, V_2O_3 presents 30 phonon branches, including seven Raman active modes ($2\ A_{1g}$; $5\ E_g$) [42]. The two A_{1g} modes for the PM phase have frequencies of ~ 7.2 THz (240 cm^{-1}) and 15 THz (500 cm^{-1}), respectively. The fitted frequency around ~ 7 THz is matching the value of the lower A_{1g} mode. This result is in agreement with previous observations of coherent phonons reported in studies performed both in PM or PI phases [27–31]. Moreover, when analyzing coherent phonon dynamics, the presence of a slight shift in the phase of the oscillations can be linked to electronic relaxation dynamics [43]. Unfortunately, the presence of several contributions near time zero does not allow an analysis to such an extent.

However, our results provide a clear monitoring of the coherent phonon dynamic across the first-order IMT transition line. In order to understand the physical picture into play, we should stress out the following points based on the variation of phonon frequency shown in Fig. 5. First, the presence of a plateaulike behavior for pressure higher than 4500 bars tends to indicate the establishment of the PM phase above this value. This statement is further supported when looking at static differential reflectivity where a change of behavior is observed around 3000 bars (Fig. 10, Appendix E). Additionally, a slight increase in the frequency of A_{1g} phonon is expected in the PM phase with increasing pressure. The fitted value, using an affine function for frequencies above 4500 bars, provides an experimental increase of +0.0075 THz per kbar for this plausible PM phase and fulfills the expected behavior of a simple solid. However, the variation in frequency for lower pressures seems quite different. Indeed, the frequency linearly decreases and reaches a minimum around 3000 bars. This feature cannot be explained by a physical picture considering only a single phonon frequency related to the sole macroscopic state of the system (PI or PM), even taking into account a variation of frequency under pressure for both phases.

In order to rationalize these experimental observations, it is relevant to consider at first the behavior of solids while subject to hydrostatic pressure. In a general frame, simple solids tend to obey the Birch-Murnaghan equation of state [44,45] that stipulates that $B = -V\frac{dP}{dV}$ is a positive constant where B denotes the elastic bulk modulus. As a consequence, in simple materials, the elastic bulk modulus increases while increasing pressure and so does the speed of sound. One additional effect is that lattice potential generally hardens under pressure, resulting in an increasing frequency for optical phonon modes. This behavior corresponds to the one observed above 4500 bars in the plausible pure PM phase.

Nonetheless, the observed decrease of frequency of the A_{1g} mode in the 0–3500 bars region does not follow this general rule as it shows a softening of phonon frequency while increasing pressure. In this pressure range, the response of the system deviates from the expectation of a simple material. However, this behavior is expected as the phonon frequency is lower in the PM phase (≈7.15 THz) compared to PI phase (≈7.5 THz) so a frequency drop has to occur during the phase transition. Such a feature is a rather distinct signature of the isostructural IMT accompanied by a large volume change.

More significant is the presence of a minimal value at 3000 bars with a clear softening of a few percent (≈7 THz). This observation can be understood within the framework of a

compressible Hubbard model developed by Hassan *et al.* [7], when applied near first-order transition lines. Within this model, lattice degrees of freedom react to the softening of electronic degrees of freedom. One consequence is the prediction of a sound velocity anomaly near transition lines that emphasizes a strong coupling between acoustic phonon branches and the electronic subsystem. This behavior was experimentally observed during a pressure driven insulator-to-metal transition in a molecular material [3] and predicted to be valid also for inorganic Mott materials such as V_2O_3. Our observations, in time-resolved fashion (Fig. 5), indicate a mode softening upon compression with the appearance of a local minimum around 3000 bars. This behavior matches very well the expected evolution of sound velocity predicted in V_2O_3 for the pressure-driven phase transition [7]. Comparing these two quantities, our results tend to reveal a correlation between the sound velocity and the optical phonons frequencies of the A_{1g} mode both in steady state and out-of-equilibrium. It indicates that one possible origin for the observed behavior of the optical phonon is the critical coupling between electronic degrees of freedom and the lattice near first-order transition lines. The occurrence of this phenomenon far from the critical end point of V_2O_3 ($T = 475$ K) also matches the theoretical predictions for equilibrium conditions. Overall, our findings are in agreement with previous studies dealing with quasiequilibrium cases and tend to validate a physical picture when lattice contribution should always be considered in the insulator-to-metal Mott transition. Furthermore, this physical picture seems to be relevant even in strongly out-of-equilibrium cases after ultrafast photoexcitation.

V. CONCLUSION

With this study, we have demonstrated the possibility of using the ultrafast spectroscopy of coherent phonons to probe the evolution of a V_2O_3 thin film across the pressure driven isostructural insulator-to-metal phase transition (IMT) occurring at room temperature. The results demonstrate that such a technique can be used to interrogate the evolution of the system in the time domain and probe the phase diagram. It can be used to track the emergence of a macroscopic phase once all degrees of freedom have equilibrated on longer time scales.

Related to the V_2O_3 system under study, the behavior of the coherent phonon frequency suggests the emergence of the paramagnetic metallic phase (PM) above 4500 bars. More interestingly, the variation in frequency at lower pressures (1–3500 bars) cannot be understood solely in the frame of a biphasic material considering only a given frequency for both PI and PM phases, even when considering the very plausible coexistence of phases during the pressure driven transition. On the contrary, this evolution reflects the critical coupling of the electronic subsystem with the lattice when approaching first-order transition lines with a sudden drop in frequency around the critical pressure, here 3000 bar. Our experimental data show that such an effect, predicted at equilibrium, is also reflected in the coherent ultrafast out-of-equilibrium response. Overall, our results suggest that the lattice contribution for Mott materials must not be neglected near transition lines regardless of dealing with equilibrium or highly excited conditions.

ACKNOWLEDGMENTS

Authors acknowledge Agence Nationale de la Recherche (ANR) for funding under Grants No. ANR-21-CE30-0011-01 CRITICLAS and No. ANR-19-CE30-0004 ELECTRO-PHONE. G.P. thanks Région Bretagne for partial PhD funding (ARED PHONONIC). This work was carried out in the frame of the International Laboratory, DYNACOM IRL University of Tokyo-CNRS-UR. Authors thank E. Pastor for careful reading and fruitful comments.

APPENDIX A: FITTING MODEL

The single wavelength time traces are fitted with the model already provided in Ref. [46]:

$$\frac{\Delta R(t)}{R_0} = \cos(B\,(t - t_{0-XPM})^2 + \phi) \times \left[A_0 \exp\left(\frac{-4\ln 2 * (t - t_{0-XPM})^2}{\tau^2}\right) - A_1 \frac{8\ln(2) * (t - t_{0-XPM})}{\tau^2} \times \exp\left(\frac{-4\ln(2) * (t - t_{0-XPM})^2}{\tau^2}\right)\right] + \left[A_{\cos}\cos(\omega(t - t_0) + \phi_0)\exp\left(-\frac{t - t_0}{\tau_d}\right) + A_{\mathrm{dec}}\exp\left(-\frac{t - t_0}{\tau_{\mathrm{dec}}}\right) + (a * t + b)\right] * H(t_0).$$

The model, considering two physical phenomena of different origin, is divided into two parts. The first one describes the evolution of cross-phase modulation (XPM) with A_0 corresponding to the amplitude of the Gaussian and A_1 the amplitude of the first derivative of the Gaussian, τ their full width half-maximum (FWHM) and $t_{0-\mathrm{XPM}}$ the time zero event of XPM signal. In addition, in the case of pump pulses shorter than 25 fs, the first cosines, which include the B constant and the phase ϕ will reproduce the fringe artifact generated around the time zero event.

The second part corresponds to an exponentially damped oscillation convoluted with an heaviside function $H(t)$, in order the mimic the coherent phonon. Here ω, ϕ_0, $A_{\cos}$, and τ_d correspond to the frequency, the phase, the amplitude, and the damping decay time, respectively. In addition, A_d and τ_{dec} represent the amplitude and decay time of an electronic relaxation. In this model, t_0 represents the time zero of the material photoresponse. Also, an additional affine function accounts for possible thermoelastic effects.

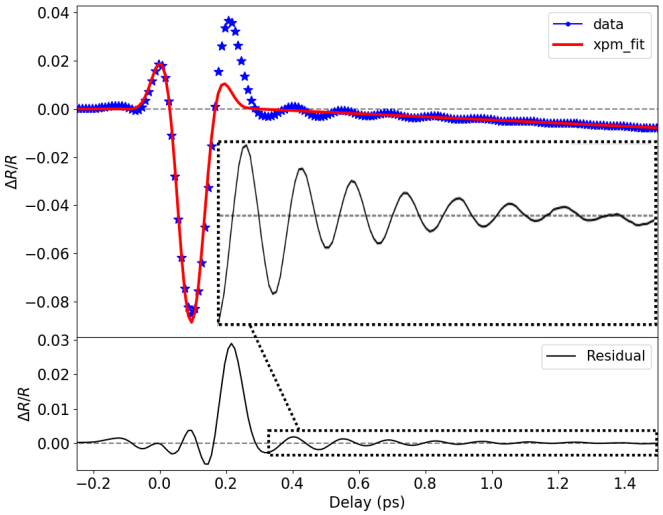

FIG. 7. (Top) Raw data and the fitted function accounting for the XPM component and thermoelastic effects. (Bottom) Residual of the signal after removal of the XPM and linear components, showing the photoresponse related to the coherent phonon (insert).

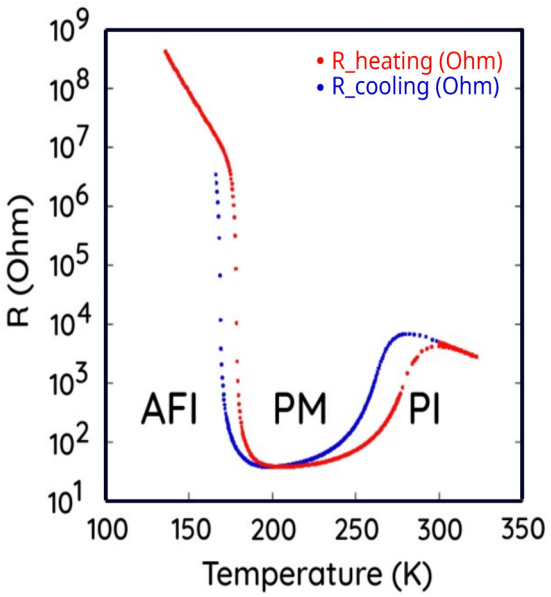

FIG. 8. Resistivity curve of the sample as a function of the temperature.

This model is taking into account cross-phase modulation (XPM) occurring when the two pulses overlap in the time domain in a dense medium, in our case the sapphire window. Different models have been then proposed to best represent the shape of the artifact using the sum of a Gaussian and its derivatives. We use the model developed by Baudisch [46], which achieves a good XPM fit by using only the first-order derivative of the Gaussian.

Figure 7 shows the experimental time trace together with the fitted part corresponding to the XPM component. It should be noticed that the asymmetric shape of the XPM component is given by the two parameters A_0 and A_1. This directly points out that the amplitude of the exponential decay that accounts for electronic relaxation A_d is strongly correlated with the XPM component as well as t_0. As can be seen in the bottom panel, the damped oscillations appear at a later time, thus avoiding a strong correlation with the other free parameters.

APPENDIX B: THERMAL BEHAVIOR OF V_2O_3 THIN FILM

The thermal behavior of the sample was monitored down to 100 K by measuring its electrical conductivity upon cooling and heating. The resistivity of the sample has been measured using the four-point probe technique. The variation of resistivity, shown in Fig. 8, reveals a double hysteresis upon heating and/or cooling with a variation of several orders of magnitude indicating the occurrence of phase transition. This feature indicates the crossing of two transition lines when cooling down the sample, starting from room temperature. Thus, the two transition temperatures T_c are: upon cooling: $T_{\text{PI–PM}} = 263$ K and $T_{\text{PM–AFI}} = 168$ K, and heating: $T_{\text{PM–PI}} = 280$ K and $T_{\text{AFI–PM}} = 178$ K.

APPENDIX C: RAMAN SPECTROSCOPY STUDY UNDER PRESSURE ON $(V_{0.962}Cr_{0.038})_2O_3$ SINGLE CRYSTAL

The Raman measurements were performed on a V_2O_3 single crystal with 3.8% of Cr substitution in the PI phase at room temperature. We used a diamond anvil cell setup [inset of Fig. 9(a)] coupled to a Renishaw confocal Raman microscope with a 785 nm excitation wavelength. Figure 9(a) compares the Raman spectra of the crystal at ambient pressure in the PI with the pressure-induced PM phases under a pressure of 17800 bars (1.7 GPa). An abrupt softening of the Raman phonons is observed at the pressure-induced PI-to-PM transition [Fig. 9(b)].

APPENDIX D: ESTIMATION OF LASER-INDUCED HEATING

We first consider a pump beam of Gaussian shape and size (BS) of ~ 290 μm FWHM. The energy of 4 μJ per pulse translates into an excitation density (ED) of ED $=\sim 2.1\,\text{mJ/cm}^2$. Afterwards, the three following interfaces at normal incidence are considered: air-sapphire, sapphire-air, and air-V_2O_3. Considering the refractive indexes of sapphire and V_2O_3 [47] at 800 nm, it comes that 79% of the incoming energy is transmitted into the V_2O_3 thin film. The excited volume of V_{exc} is $V_{\text{exc}} = \text{BS} \times 200\,\text{nm} = 3.81 \times 10^{-8}\,\text{cm}^3$. The density of deposited energy per volume is $f = \frac{\text{BS}\times\text{ED}\times 0.79}{V_{\text{exc}}} = 82.16\,\text{J/cm}^{-3}$. Based on the reported values of heat capacity for V_2O_3 [48] ($\text{Cp} = 3.25\,\text{J cm}^{-3}\,\text{K}^{-1}$), similar in both phases, we can estimate a temperature increase of about $\Delta T \approx 25$ K. We must stress that this estimated value has a physical meaning only when all degrees of freedom

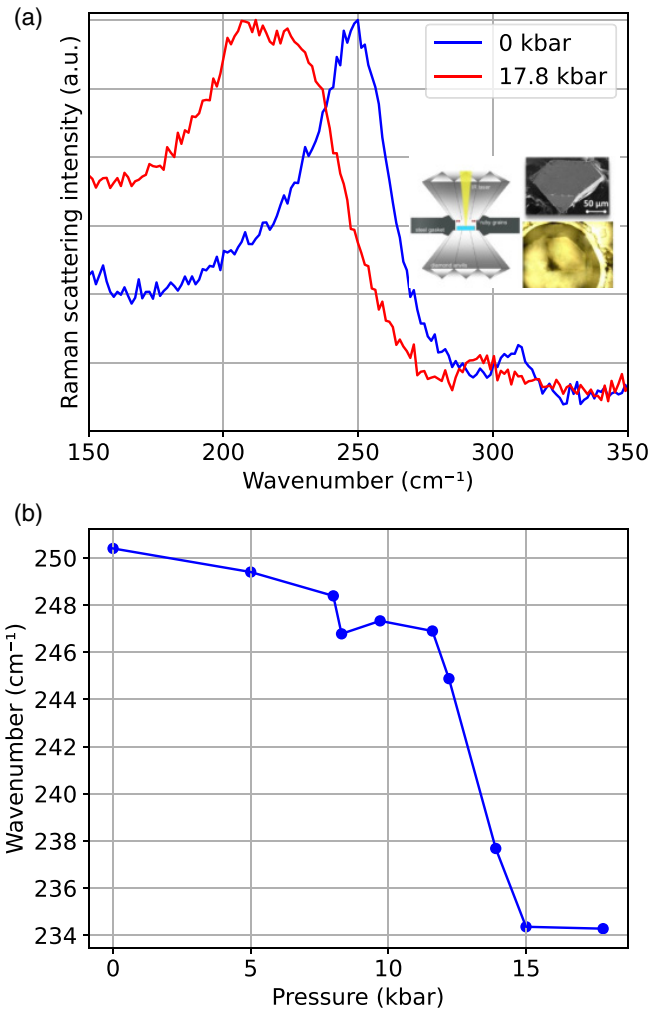

FIG. 9. (a) Comparison of Raman spectra in the metallic phases of $(V_{0.962}Cr_{0.038})_2O_3$ single crystal under a pressure of 17.8 kbar and at the ambient pressure in insulating phase at room temperature. Inset: scanning electron microscopy image of the $(V_{0.962}Cr_{0.038})_2O_3$–PI single crystal used for the Raman study under pressure and schematic illustration of the diamond anvil cell setup. (b) Evolution of the frequency of the low-energy A_{1g} mode as a function of hydrostatic pressure.

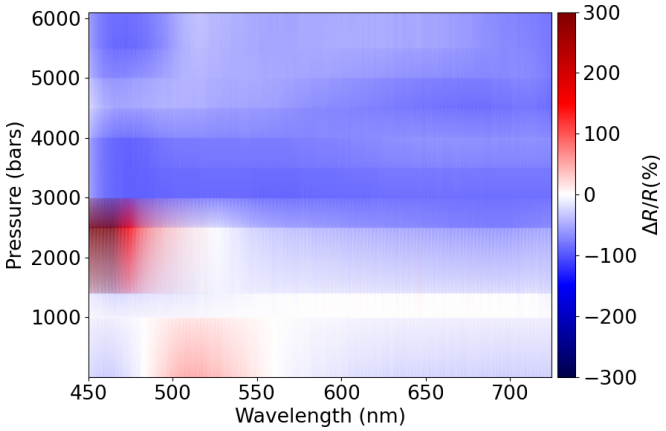

FIG. 10. Differential static reflectivity normalized with respect to the ambient pressure one as a function of pressure.

are equilibrated inside the material. It does not correspond to the lattice temperature during the ultrafast coherent response.

APPENDIX E: STEADY-STATE REFLECTIVITY OF V_2O_3 THIN FILM

Figure 10 displays the differential optical reflectivity as a function of hydrostatic pressure of the V_2O_3 thin film according to the following formula:

$$\Delta R(\lambda, P) = \frac{R_{\text{off}}(\lambda, P) - R_{\text{off}}(\lambda, P = 1\ \text{bar})}{R_{\text{off}}(\lambda, P = 1\ \text{bar})}. \qquad \text{(E1)}$$

The results indicate a change in differential reflectivity around 3000 bars, which is likely related to the change in electronic structure associated with the metallization of the sample. This feature suggests a critical pressure around 3000 bars for inducing the Mott transition. One can notice a similar trend in the change in reflectivity observed during the symmetry-breaking insulator to metal phase transition (AFI to PM) [49].

[1] N. F. Mott, Metal-insulator transition, Rev. Mod. Phys. **40**, 677 (1968).

[2] M. Imada, A. Fujimori, and Y. Tokura, Metal-insulator transitions, Rev. Mod. Phys. **70**, 1039 (1998).

[3] D. Fournier, M. Poirier, M. Castonguay, and K. D. Truong, Mott transition, compressibility divergence, and the P-T phase diagram of layered organic superconductors: An ultrasonic investigation, Phys. Rev. Lett. **90**, 127002 (2003).

[4] P. Limelette, A. Georges, D. Jérome, P. Wzietek, P. Metcalf, and J. Honig, Universality and critical behavior at the Mott transition, Science **302**, 89 (2003).

[5] E. Gati, M. Garst, R. S. Manna, U. Tutsch, B. Wolf, L. Bartosch, H. Schubert, T. Sasaki, J. A. Schlueter, and M. Lang, Breakdown of Hooke's law of elasticity at the Mott critical endpoint in an organic conductor, Sci. Adv. **2**, e1601646 (2016).

[6] M. Zacharias, L. Bartosch, and M. Garst, Mott metal-insulator transition on compressible lattices, Phys. Rev. Lett. **109**, 176401 (2012).

[7] S. R. Hassan, A. Georges, and H. R. Krishnamurthy, Sound velocity anomaly at the Mott transition: Application to organic conductors and V_2O_3, Phys. Rev. Lett. **94**, 036402 (2005).

[8] P. Majumdar and H. R. Krishnamurthy, Lattice contraction driven insulator-metal transition in the $d = \infty$ local approximation, Phys. Rev. Lett. **73**, 1525 (1994).

[9] D. B. McWhan, A. Menth, J. P. Remeika, W. F. Brinkman, and T. M. Rice, Metal-insulator transitions in pure and doped V_2O_3, Phys. Rev. B **7**, 1920 (1973).

[10] C. Tatsuyama and H. Y. Fan, Raman scattering and phase transitions in V_2O_3 and $(V_{1-x}Cr_x)_2O_3$, Phys. Rev. B **21**, 2977 (1980).

[11] D. Babich, Electron-lattice coupling at the Mott transition driven by electric and/or light pulse, Ph.D. thesis, Nantes Université, 2020.

[12] H. J. Zeiger, J. Vidal, T. K. Cheng, E. P. Ippen, G. Dresselhaus, and M. S. Dresselhaus, Theory for displacive excitation of coherent phonons, Phys. Rev. B **45**, 768 (1992).

[13] Y.-X. Yan, E. B. Gamble, Jr, and K. A. Nelson, Impulsive stimulated scattering: General importance in femtosecond laser pulse interactions with matter, and spectroscopic applications, J. Chem. Phys. **83**, 5391 (1985).

[14] G. A. Garrett, T. F. Albrecht, J. F. Whitaker, and R. Merlin, Coherent THz phonons driven by light pulses and the Sb problem: What is the mechanism? Phys. Rev. Lett. **77**, 3661 (1996).

[15] R. Merlin, Generating coherent THz phonons with light pulses, Solid State Commun. **102**, 207 (1997).

[16] K. Sokolowski-Tinten, C. Blome, J. Blums, A. Cavalleri, C. Dietrich, A. Tarasevitch, I. Uschmann, E. Förster, M. Kammler, M. Horn-von Hoegen *et al.*, Femtosecond X-ray measurement of coherent lattice vibrations near the lindemann stability limit, Nature (London) **422**, 287 (2003).

[17] G. C. Cho, W. Kütt, and H. Kurz, Subpicosecond time-resolved coherent-phonon oscillations in GaAs, Phys. Rev. Lett. **65**, 764 (1990).

[18] M. Cammarata, R. Bertoni, M. Lorenc, H. Cailleau, S. Di Matteo, C. Mauriac, S. F. Matar, H. Lemke, M. Chollet, S. Ravy, C. Laulhé, J.-F. Létard, and E. Collet, Sequential activation of molecular breathing and bending during spin-crossover photoswitching revealed by femtosecond optical and X-ray absorption spectroscopy, Phys. Rev. Lett. **113**, 227402 (2014).

[19] M. Servol, N. Moisan, E. Collet, H. Cailleau, W. Kaszub, L. Toupet, D. Boschetto, T. Ishikawa, A. Moréac, S. Koshihara, M. Maesato, M. Uruichi, X. Shao, Y. Nakano, H. Yamochi, G. Saito, and M. Lorenc, Local response to light excitation in the charge-ordered phase of $(EDO\text{-}TTF)_2SbF_6$, Phys. Rev. B **92**, 024304 (2015).

[20] H. Uemura and H. Okamoto, Direct detection of the ultrafast response of charges and molecules in the photoinduced neutral-to-ionic transition of the organic tetrathiafulvalene-*p*-chloranil solid, Phys. Rev. Lett. **105**, 258302 (2010).

[21] Y. Kawakami, S. Iwai, T. Fukatsu, M. Miura, N. Yoneyama, T. Sasaki, and N. Kobayashi, Optical modulation of effective on-site Coulomb energy for the Mott transition in an organic dimer insulator, Phys. Rev. Lett. **103**, 066403 (2009).

[22] M. Porer, U. Leierseder, J.-M. Ménard, H. Dachraoui, L. Mouchliadis, I. Perakis, U. Heinzmann, J. Demsar, K. Rossnagel, and R. Huber, Non-thermal separation of electronic and structural orders in a persisting charge density wave, Nat. Mater. **13**, 857 (2014).

[23] J. Demsar, K. Biljaković, and D. Mihailovic, Single particle and collective excitations in the one-dimensional charge density wave solid $K_{0.3}MoO_3$ probed in real time by femtosecond spectroscopy, Phys. Rev. Lett. **83**, 800 (1999).

[24] S. Mor, M. Herzog, J. Noack, N. Katayama, M. Nohara, H. Takagi, A. Trunschke, T. Mizokawa, C. Monney, and J. Stähler, Inhibition of the photoinduced structural phase transition in the excitonic insulator Ta_2NiSe_5, Phys. Rev. B **97**, 115154 (2018).

[25] T. Y. Jeong, B. M. Jin, S. H. Rhim, L. Debbichi, J. Park, Y. D. Jang, H. R. Lee, D.-H. Chae, D. Lee, Y.-H. Kim *et al.*, Coherent lattice vibrations in mono-and few-layer WSe_2, ACS Nano **10**, 5560 (2016).

[26] D. Werdehausen, T. Takayama, M. Höppner, G. Albrecht, A. W. Rost, Y. Lu, D. Manske, H. Takagi, and S. Kaiser, Coherent order parameter oscillations in the ground state of the excitonic insulator Ta_2NiSe_5, Sci. Adv. **4**, eaap8652 (2018).

[27] O. V. Misochko, M. Tani, K. Sakai, K. Kisoda, S. Nakashima, V. N. Andreev, and F. A. Chudnovsky, Optical study of the Mott transition in V_2O_3: Comparison of time-and frequency-domain results, Phys. Rev. B **58**, 12789 (1998).

[28] B. Mansart, D. Boschetto, S. Sauvage, A. Rousse, and M. Marsi, Mott transition in Cr-doped V_2O_3 studied by ultrafast reflectivity: Electron correlation effects on the transient response, Europhys. Lett. **92**, 37007 (2010).

[29] G. Lantz, B. Mansart, D. Grieger, D. Boschetto, N. Nilforoushan, E. Papalazarou, N. Moisan, L. Perfetti, V. L. Jacques, D. Le Bolloc'h *et al.*, Ultrafast evolution and transient phases of a prototype out-of-equilibrium Mott–Hubbard material, Nat. Commun. **8**, 13917 (2017).

[30] G. Huitric, M. Rodriguez-Fano, L. Gournay, N. Godin, M. Hervé, G. Privault, J. Tranchant, Z. Khaldi, M. Cammarata, E. Collet *et al.*, Impact of the terahertz and optical pump penetration depths on generated strain waves temporal profiles in a V_2O_3 thin film, Faraday Discuss. **237**, 389 (2022).

[31] A. S. Johnson, D. Moreno-Mencía, E. B. Amuah, M. Menghini, J.-P. Locquet, C. Giannetti, E. Pastor, and S. E. Wall, Ultrafast loss of lattice coherence in the light-induced structural phase transition of V_2O_3, Phys. Rev. Lett. **129**, 255701 (2022).

[32] S. W. Teitelbaum, T. Shin, J. W. Wolfson, Y.-H. Cheng, I. J. Porter, M. Kandyla, and K. A. Nelson, Real-time observation of a coherent lattice transformation into a high-symmetry phase, Phys. Rev. X **8**, 031081 (2018).

[33] S. Wall Jr, D. Wegkamp, L. Foglia, K. Appavoo, J. Nag, R. Haglund, J. Stähler, and M. Wolf, Ultrafast changes in lattice symmetry probed by coherent phonons, Nat. Commun. **3**, 721 (2012).

[34] G. Privault, G. Huitric, M. Hervé, E. Trzop, J. Tranchant, B. Corraze, Z. Khaldi, L. Cario, E. Janod, J.-C. Ameline *et al.*, Ultrafast photo-induced dynamics of V_2O_3 thin films under hydrostatic pressure, Eur. Phys. J.: Spec. Top. **232**, 2195 (2023).

[35] M. Lorenc, M. Ziolek, R. Naskrecki, J. Karolczak, J. Kubicki, and A. Maciejewski, Artifacts in femtosecond transient absorption spectroscopy, Appl. Phys. B **74**, 19 (2002).

[36] K. Ekvall, P. Van Der Meulen, C. Dhollande, L.-E. Berg, S. Pommeret, R. Naskrecki, and J.-C. Mialocq, Cross phase modulation artifact in liquid phase transient absorption spectroscopy, J. Appl. Phys. **87**, 2340 (2000).

[37] A. Bresci, M. Guizzardi, C. Valensise, F. Marangi, F. Scotognella, G. Cerullo, and D. Polli, Removal of cross-phase modulation artifacts in ultrafast pump–probe dynamics by deep learning, APL Photon. **6**, 076104 (2021).

[38] D. Boschetto, M. Weis, J. Zhang, J. Caillaux, N. Nilforoushan, G. Lantz, B. Mansart, E. Papalazarou, N. Moisan, D. Grieger *et al.*, Reply to: Ultrafast evolution and transient phases of a prototype out-of-equilibrium Mott-Hubbard material, Nat. Commun. **10**, 4035 (2019).

[39] D. Moreno-Mencía, A. Ramos-Álvarez, L. Vidas, S. M. Koohpayeh, and S. Wall, Ultrafast evolution and transient

phases of a prototype out-of-equilibrium Mott-Hubbard material, Nat. Commun. **10**, 4034 (2019).

[40] B. Arnaud and Y. Giret, Electron cooling and Debye-Waller effect in photoexcited Bismuth, Phys. Rev. Lett. **110**, 016405 (2013).

[41] L. Waldecker, T. Vasileiadis, R. Bertoni, R. Ernstorfer, T. Zier, F. H. Valencia, M. E. Garcia, and E. S. Zijlstra, Coherent and incoherent structural dynamics in laser-excited antimony, Phys. Rev. B **95**, 054302 (2017).

[42] A. Okamoto, Y. Fujita, and C. Tatsuyama, Raman study on the high temperature transition in V_2O_3, J. Phys. Soc. Jpn. **52**, 312 (1983).

[43] E. M. Bothschafter, A. Paarmann, E. S. Zijlstra, N. Karpowicz, M. E. Garcia, R. Kienberger, and R. Ernstorfer, Ultrafast evolution of the excited-state potential energy surface of TiO_2 single crystals induced by carrier cooling, Phys. Rev. Lett. **110**, 067402 (2013).

[44] F. D. Murnaghan, The compressibility of media under extreme pressures, Proc. Natl. Acad. Sci. USA **30**, 244 (1944).

[45] F. Birch, Finite elastic strain of cubic crystals, Phys. Rev. **71**, 809 (1947).

[46] B. Baudisch, Time resolved broadband spectroscopy from UV to NIR, lmu, Ph.D. thesis, 2018.

[47] C. Lamsal and N. Ravindra, Optical properties of vanadium oxides-an analysis, J. Mater. Sci. **48**, 6341 (2013).

[48] H. Keer, D. Dickerson, H. Kuwamoto, H. Barros, and J. Honig, Heat capacity of pure and doped V_2O_3 single crystals, J. Solid State Chem. **19**, 95 (1976).

[49] A. Ronchi, P. Homm, M. Menghini, P. Franceschini, F. Maccherozzi, F. Banfi, G. Ferrini, F. Cilento, F. Parmigiani, S. S. Dhesi, M. Fabrizio, J.-P. Locquet, and C. Giannetti, Early-stage dynamics of metallic droplets embedded in the nanotextured Mott insulating phase of V_2O_3, Phys. Rev. B **100**, 075111 (2019).